

Information theoretic measures of Hookium using generalized pseudo-spectral technique within density functional theory

Raveena Arya, Santanu Mondal, and Amlan K. Roy

Department of Chemical Sciences, Indian Institute of Science Education and Research (IISER) Kolkata, Mohanpur 741246, Nadia, India.

Received 24 February 2025; accepted 26 April 2025

Atomic systems subjected to external confinement exhibit a range of intriguing physical properties. In this work, we employ a well-established work-function-based Kohn-Sham density functional theory (DFT) within a generalized pseudospectral (GPS) method to determine the energy eigenvalues and eigenfunctions of Hookium (a two-electron system bound by a harmonic potential). We consider the two cases, *viz.* (i) Hookium and (ii) Hookium under the influence of a spherical cavity confinement. Two correlation energy functionals like Wigner and Lee-Yang-Parr (LYP) are considered to include explicit correlation energy in the calculation. Furthermore, we provide a comprehensive analysis of the quantum information-theoretic aspects of confined systems by examining the position-space Shannon and Fisher entropies.

Keywords: Quantum dot; harmonic confinement; Hookium; quantum information entropy; density functional theory.

DOI: <https://doi.org/10.31349/SuplRevMexFis.6.011310>

1. Introduction

The study of confined quantum systems has been a fascinating area of research since the advent of quantum mechanics. In particular, quantum dots (QDs), where particles are confined within nanoscale cavities, have emerged as a promising research frontier [1-8]. QDs have attracted considerable interest across various scientific and technological domains due to their tunable electronic properties, making them strong candidates for qubits [9]. A wide range of confinement potentials—such as harmonic, finite oscillator, rectangular, parabolic, and Woods-Saxon models—have been employed to trap electrons in QDs [3,4,10-21]. Among these, harmonic confinement stands out due to its analytical tractability and effectiveness in modeling few-electron systems, particularly two-electron configurations [22-29]. Moreover, the quadratic nature of the harmonic potential makes it a reliable approximation for describing the confinement of multiple electrons in a QD. A two-body fermionic system, such as two electrons under harmonic confinement, presents a valuable opportunity to gain deeper insights into electronic interactions. Despite the presence of a positively charged nucleus at the center, two electrons in a harmonic potential can form a bound state, leading to such systems often being referred to as *artificial atoms*. In the literature, a two-electron system under the effect of harmonic potential rather than a Coulomb potential is commonly referred to as a *harmonium* or *Hookium* atom [24,30-32]. But, here we use the term as Hookium as suggested by Pupyshev and Montgomery [24]. First, Eden and Emery [33] introduced such a model in order to study the nuclei. Extensive studies on such systems have primarily emphasized energetic properties, while relatively fewer investigations have explored quantum information characteristics [34-38]. Furthermore, the ability to externally ma-

nipulate such a system has generated significant interest in quantum information measures. These measures are often quantified using entropic descriptors such as Shannon and Fisher entropy, particularly in the context of geometrically tunable few-electron systems [36,39,40]. The Shannon entropy (S_r), which is often known as a global measure of information entropy, provides statistical information about the de-localization of the system. In contrast, Fisher entropy (I_r) popular as the local measure of the information entropy indicates the localization of a quantum system.

In this work, we investigate the properties of Hookium by solving the non-relativistic Kohn-Sham (KS) equation, which has proven to be highly effective in determining the energy spectrum of many-electron atoms. To achieve high-precision solutions for the eigenvalue equations, we employ a specialized generalized pseudospectral (GPS) method [41]. Additionally, we explore the effects of impenetrable spherical cavity confinement by placing Hookium at the center of the spherical cavity. The position-space Shannon and Fisher entropies of Hookium are then analyzed by tuning both K (the force constant) and r_c (the cavity radius). The manuscript is structured as follows: Sec. 2 provides a brief overview of the present method, followed by a detailed discussion of results in Sec. 3. Finally, our conclusions are summarized in Sec. 4.

2. Methodology

The fundamental framework of the work-function-based density functional method is first outlined for an atomic system confined by the combined influence of a harmonic potential and an impenetrable spherical cage. This is followed by a concise discussion of the GPS scheme [41], which is employed to compute the eigenvalues and eigenfunctions of the target KS equation. The starting point involves formulat-

ing the non-relativistic, single-particle, time-independent KS equation under impenetrable confinement as,

$$\hat{H}(\vec{r})\psi_i(\vec{r}) = \epsilon_i(\vec{r})\psi_i(\vec{r}), \quad (1)$$

where ψ_i and ϵ_i refer to the eigenfunction and eigenenergy corresponding to the i th orbital. Here, \hat{H} refers to the effective KS Hamiltonian, given by,

$$\begin{aligned} \hat{H}(\vec{r}) &= -\frac{1}{2}\nabla^2 + v_{eff}(\vec{r}), \\ v_{eff}(\vec{r}) &= v_{ne}(\vec{r}) + \int \frac{\rho(\vec{r}')}{|\vec{r} - \vec{r}'|} d\vec{r}' \\ &\quad + \frac{\delta E_{xc}[\rho(\vec{r})]}{\delta \rho(\vec{r})} + v_{conf}(\vec{r}), \end{aligned} \quad (2)$$

where, $v_{ne}(\vec{r})$ is the external electron-nuclear attraction potential, whereas the second and third terms in the right-hand side of the above equation represent classical Coulomb (Hartree) repulsion and XC potentials, respectively. In the above and what follows, the equations are presented in atomic units (a.u.). The confinement potential has the form,

$$v_{conf}(\vec{r}) = \begin{cases} \frac{1}{2}Kr^2, & \text{for } r \leq r_c, \\ +\infty, & \text{elsewhere.} \end{cases} \quad (3)$$

Here, K and r_c denote the force constant and radius of the spherical cavity, respectively. A highly accurate work-function-based potential, $v_x(\vec{r})$, is employed [42,43]. Using this potential, the exchange energy is evaluated by interpreting it as the interaction energy between an electron at \vec{r} and its Fermi-Coulomb hole charge density, $\rho_x(\vec{r}, \vec{r}')$, at \vec{r}' . The explicit form is given by [42,43],

$$E_x[\rho(\vec{r})] = \frac{1}{2} \int \int \frac{\rho(\vec{r})\rho_x(\vec{r}, \vec{r}')}{|\vec{r} - \vec{r}'|} d\vec{r}d\vec{r}'. \quad (4)$$

Here, we impose a specific local exchange potential, $v_x(\vec{r})$, that corresponds to a given state. Consequently, the work-function potential can be understood as the work required to bring an electron from infinity to a point \vec{r} within the electric field generated by its Fermi-Coulomb hole density. Its explicit form is given by,

$$v_x(\vec{r}) = - \int_{\infty}^{\vec{r}} \mathcal{E}_x(\vec{r}) \cdot d\vec{l}, \quad (5)$$

where

$$\mathcal{E}_x(\vec{r}) = \int \frac{\rho_x(\vec{r}, \vec{r}')(\vec{r} - \vec{r}')}{|\vec{r} - \vec{r}'|^3} d\vec{r}'. \quad (6)$$

The electron density is evaluated in terms of occupied orbitals M , as,

$$\rho(\vec{r}) = \sum_{i=1}^M n_i |\psi_i(\vec{r})|^2. \quad (7)$$

where n_i denotes the number of electrons in the i th orbital, while M is the number of electrons in the system.

In this work, to account exchange only case, we use the above $v_x(\vec{r})$, while the correlation effect is underscored with

simple Wigner [44] and slightly involved LYP [45] energy functionals. Therefore, we solve the KS equation in a self-consistent manner. The adaptation of the GPS method for the accurate and efficient solution of the KS equation results in a non-uniform, optimally spaced spatial discretization. The present method relies on approximating an *exact* function $f(x) \in [-1, 1]$ with the help of a N th-order polynomial $f_N(x)$ as,

$$f(x) \cong f_N(x) = \sum_{j=0}^N f(x_j)g_j(x), \quad (8)$$

in a way such that,

$$f_N(x_j) = f(x_j), \quad (9)$$

and it signifies that each of our estimation points is precise at the collocation point. Due to the impenetrable nature of the spherical cavity of radius r_c , we expand the radial region within the range $[0, r_c]$. Therefore, we have mapped r_c ($r \in [0, r_c]$) onto the interval $[-1, 1]$ by utilizing a non-linear mapping function,

$$r = r(x) = L \frac{1+x}{1-x+\alpha}, \quad (10)$$

where, L and $\alpha = 2L/r_c$ refer to two mapping parameters.

In the Legendre pseudo-spectral method, x_0 and x_N take the values of -1 and 1 , respectively, while all other roots x_j ($j = 1, \dots, N-1$) are determined from the first-order derivative of the Legendre polynomial $P_N(x)$ following the equation,

$$P'_N(x_j) = 0. \quad (11)$$

The cardinal functions $g_j(x)$ (see Eq. (8)) are evaluated from,

$$g_j(x) = -\frac{1}{N(N+1)P_N(x_j)} \frac{(1-x^2)P'_N(x)}{(x-x_j)}, \quad (12)$$

which satisfy the condition

$$g_j(x_{j'}) = \delta_{j',j}. \quad (13)$$

Hence, we end up with a symmetric eigenvalue problem, which is then solved by standard software to accurately determine the eigenvalues and eigenfunctions of a system (F02BBF from NAG Fortran Library Routine [46]). For further in-depth calculation, we refer the reader to go through [47-51] and references therein.

The impenetrable nature of the spherical cavity on the system is achieved by ensuring the total electron density dissipates at the cavity boundary, and it satisfies the Dirichlet boundary condition $\psi_{nl}(0) = \psi_{nl}(r_c) = 0$. Equation (7) follows the normalization criterion,

$$\int \rho(\vec{r}) d\vec{r} = M. \quad (14)$$

All calculations are done with unit-normalized density. The explicit knowledge of unit-normalized density $\tilde{\rho}(\vec{r})$ is used to quantify the Shannon entropy and Fisher entropy following the definitions,

$$S_r = - \int \tilde{\rho}(\vec{r}) \ln[\tilde{\rho}(\vec{r})] d\vec{r}, \quad (15)$$

and

$$I_r = \int \frac{|\nabla \tilde{\rho}(\vec{r})|^2}{\tilde{\rho}(\vec{r})} d\vec{r}. \quad (16)$$

All calculations in this report are carried out numerically, ensuring convergence by systematically varying grid parameters, including the total number of radial points and the maximum grid range. Notably, convergence is achieved more readily in regions of lower r_c or higher K , whereas it becomes a little bit tricky as the system approaches the free-space limit ($r_c \rightarrow \infty$). All data reported in this work are checked rigorously through a convergence test. A general convergence criteria in energy (10^{-6}) and potential (10^{-5}) during the iterative process were employed throughout the whole confinement region.

3. Results and discussion

Here, we represent the ground state energy of a two-electron system under impenetrable harmonic confinement. We are confining the system by varying the radius cavity r_c and force constant K . In Table I the total energy is shown with different grid points for convergence purposes for X-Only and XC-Wigner. Here the convergence can be seen up to four decimal places.

In Table II the total energy is shown, where X-only represents near-Hartree-Fock energy, and exchange with correlation energy is modeled by XC-Wigner functional and XC-LYP functional. The present results are in good agreement with Ref. [29]. In this work, we have utilized the Ritz variational method with an explicitly correlated multi-exponent Hylleraas basis to calculate the ground state energy of Hookium in the free limit of $r_c \rightarrow \infty$. For instance, it is reported that E_{XC} is 2.72617 at $K = 0.5$, while the values of the same are 2.74 and 2.73 for the Wigner and LYP correlation functional.

The qualitative nature of the two-electron Hookium atom is shown in the given plots. In Fig. 1a) represents the variation of energy E as a function of force constant K , in which

TABLE I. Energy E of the Hookium atom as a function of r_c and K for different grid points (N). All quantities are in a.u.

r_c	K	E									
		X-only					XC-Wigner				
		$N = 100$	$N = 200$	$N = 250$	$N = 300$	$N = 350$	$N = 100$	$N = 200$	$N = 250$	$N = 300$	$N = 350$
0.2	0.5	255.6625	255.6619	255.6618	255.6618	255.6618	255.5211	255.5205	255.5204	255.5204	255.5204
	5	255.7136	255.7131	255.7130	255.7130	255.7130	255.5722	255.5717	255.5716	255.5716	255.5716
1	0.5	11.7868	11.7867	11.7866	11.7866	11.7866	11.7223	11.7221	11.7221	11.7221	11.7221
	5	13.0668	13.0666	13.0666	13.0666	13.0666	13.0015	13.0014	13.0014	13.0014	13.0014
10	0.5	2.7664	2.7662	2.7662	2.7662	2.7662	2.7379	2.7377	2.7377	2.7377	2.7377
	5	7.8747	7.8744	7.8744	7.8744	7.8744	7.8282	7.8280	7.8279	7.8279	7.8279

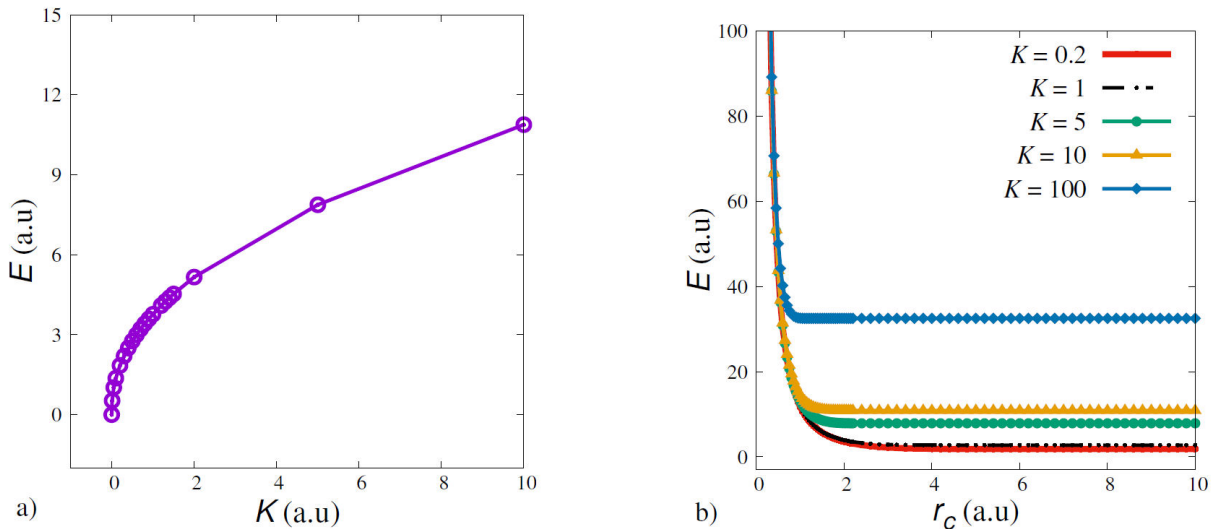


FIGURE 1. Energy E of the Hookium atom as a function of K and r_c .

TABLE II. Energy E of Hookium atom as a function of r_c and K . All quantities are in a.u.

r_c	K	E		
		X-only	XC-Wigner	XC-LYP
0.2	0.5	255.6618	255.5204	256.2546
	1.0	255.6675	255.5261	256.2602
	5.0	255.7130	255.5716	256.3057
	10.0	255.7699	255.6285	256.3625
	100.0	256.7925	256.6511	257.3839
0.5	0.5	43.0722	42.9746	43.2880
	1.0	43.1080	43.0104	43.3237
	5.0	43.3942	43.2965	43.6092
	10.0	43.7512	43.6534	43.9651
	100.0	50.0310	49.9323	50.2286
1.0	0.5	11.7866	11.7221	11.8460
	1.0	11.9311	11.8664	11.9899
	5.0	13.0666	13.0014	13.1212
	10.0	14.4386	14.3726	14.4883
	100.0	32.5615	32.4828	32.5904
5.0	0.5	2.7662	2.7377	2.7322
	1.0	3.7715	3.7383	3.7395
	5.0	7.8744	7.8279	7.8536
	10.0	10.8786	10.8255	10.8656
	100.0	32.4956	32.4171	32.5208
10.0	0.5	2.7662	2.7377	2.7322
	1.0	3.7715	3.7383	3.7395
	5.0	7.8744	7.8279	7.8536
	10.0	10.8786	10.8255	10.8656
	100.0	32.4956	32.4171	32.5208
100.0	0.5	2.7662	2.7377	2.7322
	1.0	3.7715	3.7383	3.7395
	5.0	7.8744	7.8279	7.8536
	10.0	10.8786	10.8255	10.8656
	100.0	32.4956	32.4171	32.5208

the energy increases monotonically with K , implying that the system goes to a high energy level under strong confinement. In Fig. 1b) shows how the energy E varies with r_c at fixed values of K . For weaker confinement K , energy decreases significantly as the radius of cavity r_c increases. When $r_c \lesssim 2$, the energy gradually increases. Whereas, for larger K , the energy demonstrates minimal dependence on r_c and persists relatively very high. Hence, we can observe that the effect of the radius cavity is negligible when the harmonic potential dominates. This behavior is crucial in understanding quantum confinement effects in nanoscale devices, such as quantum dots, where both external potential and spatial boundaries determine electronic properties.

The information-theoretic study further helps to understand these observations in a more effective way. Table III reports S_r and I_r for the ground state of Hookium under

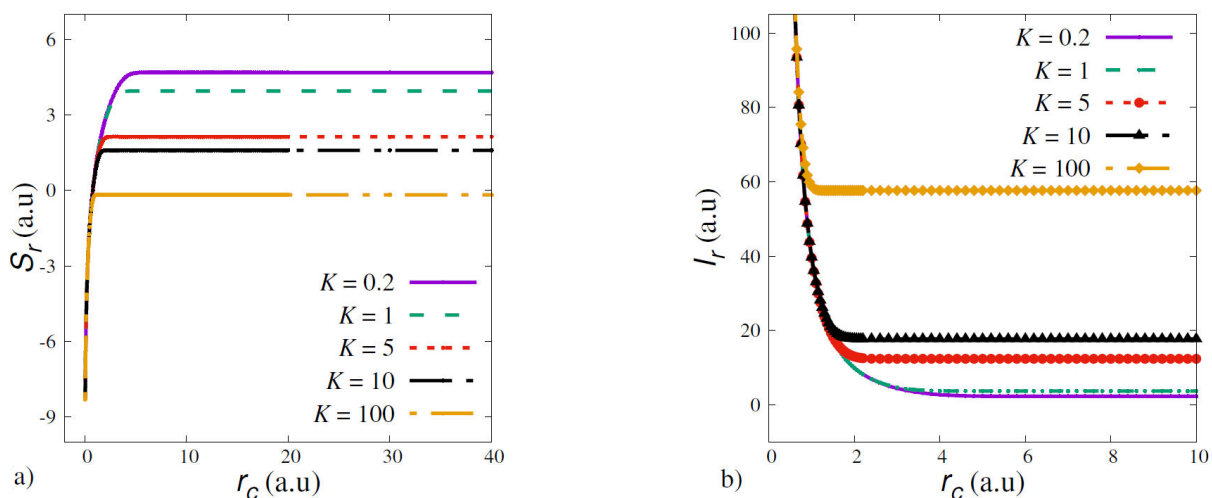
confinement. The values of S_r and I_r for the X-only, XC-Wigner, and XC-LYP approximations exhibit subtle differences for small cavity radii $r_c \lesssim 5$ but start to show differences for larger cavities $r_c \gtrsim 5$. Also, it shows the variation of the force constant K . This behavior brings attention to the role of correlation effects in the system and the effect of harmonic confinement on electron distribution in the absence of a central positive charge.

For small cavity sizes $r_c \lesssim 5$, the external harmonic potential dominates, forcing the electrons into a highly localized region. Under such strong confinement, the electron density remains sharply peaked, and correlation effects are suppressed. As a result, the electron density distributions obtained from X-only, XC-Wigner, and XC-LYP approximations are nearly identical, with S_r and I_r differing only slightly beyond the third decimal place. Since the electrons have limited spatial freedom, their ability to rearrange due to mutual repulsion is constrained, meaning that exchange interactions alone (X-only) are sufficient to describe the system, without significant correlation corrections.

However, as the radius cavity size increases beyond $r_c \gtrsim 5$, the electron cloud tends to spread more, allowing electron-electron repulsion to play a more significant role in shaping the density distribution. In this regime, due to higher uncertainty in electron positions, the system indicates delocalization. Hence, S_r interprets increased nature. Meanwhile, localization of the system decreases, resulting in a decline in I_r . The appearance of differences between X-only and XC functionals in this region indicates that correlation effects become important when confinement weakens. In Fig. 2a) S_r varies with respect to the cavity radius r_c for different fixed values of K . The results demonstrate that for small K , S_r increases as r_c increases. This increase implies the rising spatial delocalization of the electron density, as a larger radius cavity allows us to spread more of the electronic cloud. When confinement is weak, the probability distribution extends over a broader spatial region, leading to a higher uncertainty in electron position, which corresponds to an increase in S_r . For large K , however, S_r remains relatively low even as r_c increases. The stronger harmonic potential restricts the electrons to a well-defined region, suppressing delocalization. In this regime, the spatial confinement imposed by the harmonic potential is more dominant than the finite size of the cavity, leading to a localized electron density with lower S_r . Therefore, S_r serves as a measure of the balance between delocalization due to spatial freedom and localization due to confinement strength. In Fig. 2b), I_r changes with cavity radius r_c for different fixed values K . Note that I_r measures localization, meaning higher values indicate a more sharply confined electron density, while lower values suggest a more spread-out distribution. In the low regime of r_c , I_r increases rapidly, signifying that the system is highly localized in this region. In the low regime of r_c the system experiences strong confinement, which restricts the electron in a highly localized area. Due to the enhancement of localization, the electron density distribution becomes highly structured, which leads

TABLE III. S_r (a.u.) and I_r (a.u.) in the ground state of Hookium.

r_c	K	S_r			I_r		
		X-only	XC-Wigner	XC-LYP	X-only	XC-Wigner	XC-LYP
0.2	0.5	-4.15	-4.15	-4.15	987.02	987.02	987.02
	1	-4.15	-4.15	-4.15	987.02	987.02	987.02
	5	-4.15	-4.15	-4.15	987.01	987.01	987.01
	10	-4.15	-4.15	-4.15	987.01	987.01	987.01
	100	-4.15	-4.15	-4.15	986.99	986.99	986.99
0.5	0.5	-1.39	-1.39	-1.39	157.97	157.97	157.97
	1	-1.39	-1.39	-1.39	157.96	157.96	157.96
	5	-1.39	-1.39	-1.39	157.95	157.95	157.95
	10	-1.39	-1.39	-1.39	157.94	157.94	157.94
	100	-1.45	-1.45	-1.45	158.25	158.25	158.25
1	0.5	0.70	0.70	0.70	39.52	39.52	39.52
	1	0.70	0.70	0.70	39.51	39.50	39.51
	5	0.66	0.66	0.66	39.49	39.49	39.49
	10	0.61	0.61	0.61	39.65	39.65	39.65
	100	-0.20	-0.20	-0.20	58.77	58.81	58.78
5	0.5	3.95	3.94	3.95	3.68	3.71	3.69
	1	3.40	3.39	3.40	5.31	5.35	5.32
	5	2.14	2.13	2.13	12.34	12.39	12.35
	10	1.60	1.59	1.60	17.68	17.73	17.69
	100	-0.18	-0.18	-0.18	57.63	57.67	57.64
10	0.5	3.95	3.94	3.95	3.68	3.71	3.69
	1	3.40	3.39	3.40	5.31	5.35	5.32
	5	2.14	2.13	2.13	12.35	12.39	12.36
	10	1.60	1.59	1.60	17.68	17.73	17.69
	100	-0.18	-0.18	-0.18	57.63	57.68	57.64
100	0.5	3.95	3.94	3.95	3.68	3.71	3.69
	1	3.40	3.39	3.40	5.32	5.35	5.33
	5	2.13	2.13	2.13	12.35	12.39	12.36
	10	1.60	1.59	1.60	17.69	17.73	17.69
	100	-0.18	-0.18	-0.18	57.64	57.68	57.64


 FIGURE 2. Shannon entropy S_r and Fisher information I_r of the Hookium atom as a function of r_c .

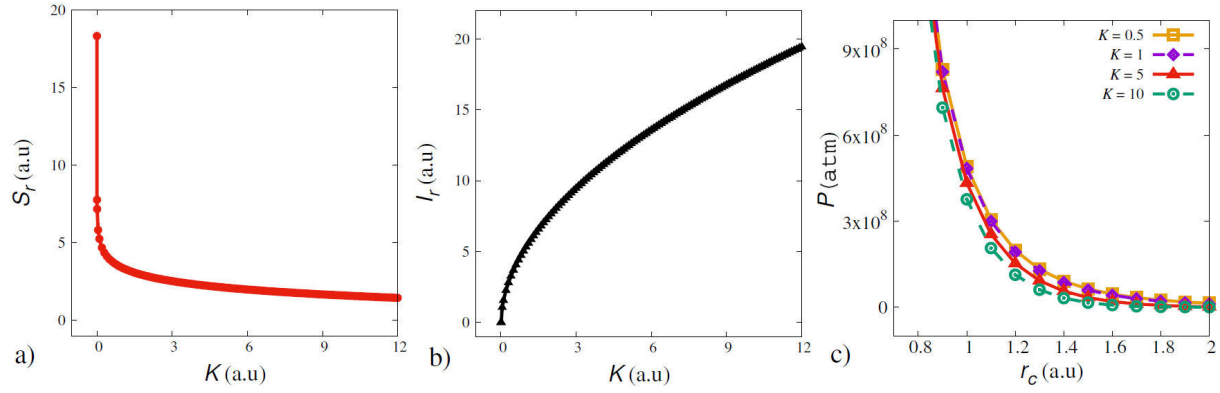


FIGURE 3. Panels a) and b) show the Shannon entropy S_r and Fisher information I_r of the Hookium atom as a function of K in the free limit of r_c . Panel c) shows variation of Pressure (in atm) with r_c and with different K .

TABLE IV. Pressure P (in atm) in the ground state of the Hookium atom as a function of r_c and K .

r_c	K	P		
		X-only	XC-Wigner	XC-LYP
0.2	0.5	1.45(+12)	1.45(+12)	1.45(+12)
	1	1.45(+12)	1.45(+12)	1.45(+12)
	5	1.45(+12)	1.45(+12)	1.45(+12)
	10	1.45(+12)	1.45(+12)	1.45(+12)
0.3	0.5	1.93(+11)	1.93(+11)	1.93(+11)
	1	1.93(+11)	1.93(+11)	1.93(+11)
	5	1.93(+11)	1.93(+11)	1.93(+11)
0.5	10	1.92(+11)	1.92(+11)	1.93(+11)
	0.5	1.52(+10)	1.52(+10)	1.53(+10)
	1	1.52(+10)	1.52(+10)	1.53(+10)
1	5	1.51(+10)	1.51(+10)	1.52(+10)
	10	1.50(+10)	1.50(+10)	1.50(+10)
	0.5	4.91(+8)	4.90(+8)	4.94(+8)
2	1	4.84(+8)	4.83(+8)	4.88(+8)
	5	4.33(+8)	4.32(+8)	4.37(+8)
	10	3.76(+8)	3.75(+8)	3.80(+8)
2	0.5	1.36(+7)	1.35(+7)	1.38(+7)
	1	1.09(+7)	1.08(+7)	1.11(+7)
	5	1.66(+6)	1.64(+6)	1.72(+6)
	10	1.70(+5)	1.68(+5)	1.79(+5)

to a sharp rise in I_r . As r_c increases, I_r starts to decline, which highlights the picture of the dominating behavior of the delocalization, and the density distribution is becoming smoother.

As K increases, the harmonic potential dominates, pulling the electrons toward the center and making the density more concentrated, which raises I_r .

Furthermore, Fig. 3 shows S_r and I_r variation with force constant K in the free limit. In Fig. 3a), the effect of confinement on the electron density now comes solely from K . As K increases, S_r decreases, indicating that the system be-

comes more localized when K increases. When K is small, the electron cloud spread is wider, tending to S_r , and rises sharply for $K \lesssim 3$ due to increased positional uncertainty. As K increases, the harmonic potential becomes stronger. Hence, the confinement effect on the system increases the sharpness or concentration of the electronic charge density. The decreasing nature of S_r reflects that the electron density shrinks as K increases, *i.e.*, it shows that the system is becoming localized for a stronger confinement regime. In Fig. 3b) presents the variation of I_r with K . I_r increases monotonically as K increases, which indicates that a stronger

harmonic confinement enhances localization. Therefore, I_r serves as a direct measure of how sharply localized the electronic distribution is. Since I_r exhibits the property of localization of the system, its increase with K confirms that the system becomes more confined for the strong harmonic potential. The system is more delocalized for smaller values of K . Overall, there is a clear interplay between cavity radius r_c and K in determining localization. The system becomes more localized when r_c decreases and K increases, as both stronger external confinement and a smaller available space force the electrons into a compact region. On the contrary, when r_c increases and K decreases, the electron cloud spread increases, which yields delocalization.

Additionally, we have estimated the thermodynamic pressure experienced by the Hookium atom utilizing the first law of thermodynamics. Under an adiabatic approximation, the pressure can be expressed as [52],

$$P = -\frac{1}{4\pi r_c^2} \frac{dE}{dr_c}. \quad (17)$$

To evaluate the numerical derivative in the above equation, we use the finite difference method, implemented by the `numpy.gradient` function of Python. Moreover, we have taken $\Delta r_c = 10^{-5}$ and calculated the corresponding ΔE around a particular r_c to estimate the pressure inside the cavity, which is shown in Table IV. A detailed variation of the same is illustrated in Fig. 3c) of Fig. 3. We note that the pressure increases monotonically as we go to the strong confinement regime ($r_c \rightarrow 0$) as well as with the increase of K .

4. Conclusions

We employ a simple work-function-based Kohn-Sham model to investigate the ground state of the Hookium atom using an accurate GPS method for the spatial discretization. Additionally, we examine the effect of an impenetrable spherical cavity of varying radius (r_c) on the energy and information entropy (S_r and I_r) of the Harmonium atom. Our results reveal that the ground state energy of the Hookium atom increases quadratically as K increases for a large cavity radius ($r_c \rightarrow \infty$). For smaller r_c , the energy sharply decreases for $r_c \lesssim 2$, but remains constant for larger r_c . As K increases, the energy curve shifts to more positive values. Both S_r and I_r indicate that for smaller r_c , the system becomes more squeezed at constant K , while for $r_c \rightarrow \infty$, the system becomes more localized as K increases. We hope that this work enhances our understanding of confined atomic systems and lays the foundation for the quantum information theory of such systems.

Acknowledgments

AKR acknowledges partial support from SERB, New Delhi (sanction order CRG/2023/004463). RA thanks CSIR-UGC, Govt. of India, for the financial support.

1. A. Franciosi and C. G. Van de Walle, Heterojunction band offset engineering, *Surf. Sci. Rep.* **25** (1996) 1, [https://doi.org/10.1016/0167-5729\(95\)00008-9](https://doi.org/10.1016/0167-5729(95)00008-9)
2. G. Schedelbeck *et al.*, Coupled Quantum Dots Fabricated by Cleaved Edge Overgrowth: From Artificial Atoms to Molecules, *Science* **278** (1997) 1792, <https://doi.org/10.1126/science.278.5344.1792>.
3. C. M. Lee, C. C. Lam, and S. W. Gu, Polarization effect on low-lying energy spectrum of two electrons bound to a Coulomb impurity in a quantum dot, *Phys. Rev. B* **61** (2000) 10376, <https://doi.org/10.1103/PhysRevB.61.10376>.
4. R. K. Pandey, M. K. Harbola, and V. A. Singh, Helium-like donors in semiconductor quantum dots, *J. Phys.: Cond. Matt.* **16** (2004) 1769, <https://doi.org/10.1088/0953-8984/16/10/009>.
5. X. Michalet *et al.*, Quantum dots for live cells, in vivo imaging, and diagnostics, *Science* **307** (2005) 538, <https://doi.org/10.1126/science.1104274>.
6. Y. C. Cao, Impurities Enhance Semiconductor Nanocrystal Performance, *Science* **332** (2011) 48, <https://doi.org/10.1126/science.1203702>.
7. C. Belver, J. Bedia, and J. Rodriguez, Titania-clay heterostructures with solar photocatalytic applications, *App. Cat. B: Env.* **176-177** (2015) 278, <https://doi.org/10.1016/j.apcatb.2015.04.004>
8. T. V. Bezyazhynaya *et al.*, Light emitting diode-photodiode optoelectronic pairs based on the InAs/InAsSb/InAsSbP heterostructure for the detection of carbon dioxide, *Semiconductors* **49** (2015) 980, <https://doi.org/10.1134/S1063782615070052>.
9. M. A. Nielsen and I. L. Chuang, Quantum Computation and Quantum Information (Cambridge University Press, 2010), <https://doi.org/10.1017/CBO9780511976667>.
10. S. R. Gadre, Information entropy and Thomas-Fermi theory, *Phys. Rev. A* **30** (1984) 620, <https://doi.org/10.1103/PhysRevA.30.620>.
11. R. J. Yáñez, W. Van Assche, and J. S. Dehesa, Position and momentum information entropies of the D-dimensional harmonic oscillator and hydrogen atom, *Phys. Rev. A* **50** (1994) 3065, <https://doi.org/10.1103/PhysRevA.50.3065>.
12. E. Kasapoglu, H. Sari, and I. Sökmen, The effect of hydrostatic pressure on optical transitions in quantum-well wires, *Physica B Cond. Matt.* **353** (2004) 345, <https://doi.org/10.1016/j.physb.2004.10.021>.
13. P. Winkler, Electron interaction in weakly confining quantum dot potentials, *Int. J. Quant. Chem.* **100** (2004) 1122, <https://doi.org/10.1002/qua.20249>.

14. P. Kimani, P. Jones, and P. Winkler, Correlation studies in weakly confining quantum dot potentials, *Int. J. Quant. Chem.* **108** (2008) 2763, <https://doi.org/10.1002/qua.21827>.
15. M. Sahin, Third-order nonlinear optical properties of a one- and two-electron spherical quantum dot with and without a hydrogenic impurity, *J. App. Phys.* **106** (2009) 063710, <https://doi.org/10.1063/1.3225100>.
16. M. Genkin and E. Lindroth, Effects of screened Coulomb impurities on autoionizing two-electron resonances in spherical quantum dots, *Phys. Rev. B* **81** (2010) 125315, <https://doi.org/10.1103/PhysRevB.81.125315>.
17. S. Chakraborty and Y. K. Ho, Autoionization resonance states of two-electron atomic systems with finite spherical confinement, *Phys. Rev. A* **84** (2011) 032515, <https://doi.org/10.1103/PhysRevA.84.032515>.
18. Z. Parang, A. Keshavarz, and N. Zamani, Optimization of optical absorption coefficient in double modified Pöschl-Teller quantum wells, *J. Comp. Elec.* **13** (2014) 1020, <https://doi.org/10.1007/s10825-014-0625-5>
19. J. K. Saha, S. Bhattacharyya, and T. Mukherjee, Electronic Structure of Helium Atom in a Quantum Dot*, *Comm. Theo. Phys.* **65** (2016) 347, <https://doi.org/10.1088/0253-6102/65/3/347>.
20. J. K. Saha, S. Bhattacharyya, and T. K. Mukherjee, Two-electron atoms under spatially compressed Debye plasma, *Phys. Plas.* **23** (2016) 092704, <https://doi.org/10.1063/1.4962508>.
21. M. C. Onyeaju *et al.*, Linear and Nonlinear Optical Properties in Spherical Quantum Dots: Generalized Hulthén Potential, *Few-Body Syst.* **57** (2016) 793, <https://doi.org/10.1007/s00601-016-1110-4>.
22. M. Moshinsky, *The Harmonic Oscillator in Modern Physics: From Atoms to Quarks* (Gordon and Breach, London, 1969).
23. R. J. Eden, V. J. Emery, and N. F. Mott, The binding energies of atomic nuclei I. Introduction and general method, *Proc. Royal Soc. London. Series A. Math. Phys. Sci.* **248** (1958) 266, <https://doi.org/10.1098/rspa.1958.0243>.
24. V. I. Pupyshev and H. E. Montgomery Spherically symmetric states of Hookium in a cavity, *Physica Scr.* **90** (2015) 085401, <https://doi.org/10.1088/0031-8949/90/8/085401>.
25. D. Bielinska-Waz, J. Karwowski, and G. Diercksen, Spectra of confined two-electron atoms, *J. Phys. B* **34** (2001) 1987, <https://doi.org/10.1088/0953-4075/34/10/312>.
26. T. Sako and G. H. F. Diercksen, Confined quantum systems: dipole polarizability of the two-electron quantum dot, the hydrogen negative ion and the helium atom, *J. Phys. B* **36** (2003) 3743, <https://doi.org/10.1088/0953-4075/36/18/304>.
27. V. V. Bobrikov and V. I. Pupyshev, Isotope effects for molecules in a cavity, *Russian Chem. Bull.* **54** (2005) 55, <https://doi.org/10.1007/s11172-005-0216-5>.
28. P. A. Maksym and T. Chakraborty, Quantum dots in a magnetic field: Role of electron-electron interactions, *Phys. Rev. Lett.* **65** (1990) 108, <https://doi.org/10.1103/PhysRevLett.65.108>.
29. A. Hazra *et al.*, Structural modifications of two-electron systems under isotropic harmonic confinement, *Eur. Phys. J. D* **75** (2021) 186, <https://doi.org/10.1140/epjd/s10053-021-00196-3>.
30. J. Cioslowski and K. Pernal, The ground state of harmonium, *The Journal of Chemical Physics* **113** (2000) 8434, <https://doi.org/10.1063/1.1318767>.
31. D. P. O'Neill and P. M. W. Gill, Wave functions and two-electron probability distributions of the Hooke's-law atom and helium, *Phys. Rev. A* **68** (2003) 022505, <https://doi.org/10.1103/PhysRevA.68.022505>.
32. P-F. Loos, Hooke's law correlation in two-electron systems, *Phys. Rev. A* **81** (2010) 032510, <https://doi.org/10.1103/PhysRevA.81.032510>.
33. R. J. Eden, V. J. Emery, and N. F. Mott, The binding energies of atomic nuclei I. Introduction and general method, *Proceedings of the Royal Society of London. Series A. Mathematical and Physical Sciences* **248** (1958) 266,
34. C. Martínez-Flores, Shannon entropy and Fisher information for endohedral confined one- and two-electron atoms, *Phys. Lett. A* **386** (2021) 126988, <https://doi.org/10.1016/j.physleta.2020.126988>.
35. N. Mukherjee, C. N. Patra, and A. K. Roy, Confined hydrogenlike ions in plasma environments, *Phys. Rev. A* **104** (2021) 012803, <https://doi.org/10.1103/PhysRevA.104.012803>
36. S. Mondal *et al.*, Stability of a two-electron system under pressure confinement: structural and quantum information theoretical analysis, *J. Phys. B* **56** (2023) 155001, <https://dx.doi.org/10.1088/1361-6455/ace177>.
37. S. Mondal *et al.*, Information-theoretic measures and Compton profile of H atom under finite oscillator potential, *J. Phys. B: At. Mol. Opt. Phys.* **57** (2024) 175001, <https://doi.org/10.1088/1361-6455/ad5fd3>.
38. C. R. Estanón *et al.*, Crámer-Rao complexity of the two-dimensional confined hydrogen, arXiv (2020)
39. S. Mondal, S. K. Nayek, and J. K. Saha, Ground and doubly excited states of He atom in non-ideal classical plasmas: structural, entanglement and information theoretical measures, *Eur. Phys. J. Plus* **137** (2022) 373, <https://doi.org/10.1140/epjp/s13360-022-02574-1>.
40. S. Mondal, K. D. Sen, and J. K. Saha, He atom in a quantum dot: Structural, entanglement, and information-theoretical measures, *Phys. Rev. A* **105** (2022) 032821, <https://doi.org/10.1103/PhysRevA.105.032821>.
41. G. Yao and S.-I. Chu, Generalized pseudospectral methods with mappings for bound and resonance state problems, *Chem. Phys. Lett.* **204** (1993) 381, [https://doi.org/10.1016/0009-2614\(93\)90025-V](https://doi.org/10.1016/0009-2614(93)90025-V).
42. V. Sahni and M. K. Harbola, Quantum-Mechanical interpretation of the local many-body potential of density-functional theory, *Int. J. Quantum Chem.* **38** (1990) 569, <https://doi.org/10.1002/qua.560382456>.

43. V. Sahni, Y. Li, and M. K. Harbola, Atomic structure in the Pauli-correlated approximation, *Phys. Rev. A* **45** (1992) 1434, <https://doi.org/10.1103/PhysRevA.45.1434>.
44. G. Brual, Gregorio and S. M. Rothstein, Rare gas interactions using an improved statistical method, *J. Chem. Phys.* **69** (1978) 1177, <https://doi.org/10.1063/1.436705>.
45. C. Lee, W. Yang, and R. G. Parr, Development of the Colle-Salvetti correlation-energy formula into a functional of the electron density, *Phys. Rev. B* **37** (1988) 785, <https://doi.org/10.1103/PhysRevB.37.785>.
46. K. McDonald, The NAG Numerical PVM Library, In J. Don-
garra, K. Madsen, and J. Waśniewski, eds., Applied Parallel Computing Computations in Physics, Chemistry and Engineering Science, **vol. 1041** of Lecture Notes in Computer Science (Springer, 1996) pp. 419-428, https://doi.org/10.1007/3-540-60902-4_44.
47. A. K. Roy and S.-I. Chu, Density-functional calculations on singly and doubly excited Rydberg states of many-electron atoms, *Phys. Rev. A* **65** (2002) 052508, <https://doi.org/10.1103/PhysRevA.65.052508>.
48. A. K. Roy, Studies on the hollow states of atomic lithium using a density functional approach, *J. Phys. B: At. Mol. Opt. Phys.* **37** (2004) 4369, <https://doi.org/10.1088/0953-4075/37/21/010>.
49. A. K. Roy, Density functional studies on the hollow resonances in the Li-isoelectronic sequence ($Z = 4-10$), *J. Phys. B: At. Mol. Opt. Phys.* **38** (2005) 1591, <https://doi.org/10.1088/0953-4075/38/11/002>.
50. A. K. Roy, Calculation of the spiked harmonic oscillators through a generalized pseudospectral method, *Phys. Lett. A* **321** (2004) 231, <https://doi.org/10.1016/j.physleta.2003.12.037>.
51. A. K. Roy, Calculation of the bound states of power-law and logarithmic potentials through a generalized pseudospectral method, *J. Phys. G: Nucl. Part. Phys.* **30** (2004) 269, <https://doi.org/10.1088/0954-3899/30/3/003>.
52. K. D. Chakladar *et al.*, Quantum-information-theoretic analysis of Zee systems under pressure confinement, *Phys. Rev. A* **110** (2024) 042819, <https://doi.org/10.1103/PhysRevA.110.042819>.